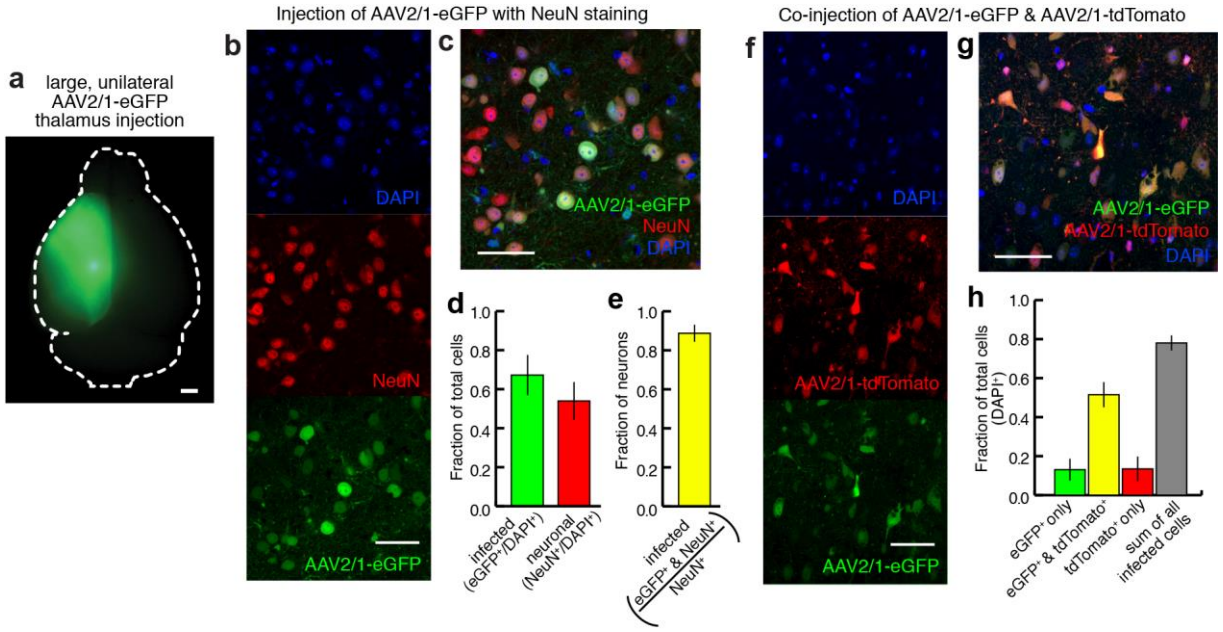

Supplementary Figure 1

Characterization of viral injections.

(a**)** Dorsal view of a mouse brain (dashed white outline) after receiving a large, unilateral thalamic injection (~100 nL); demonstrating that thalamic projections do not cross the midline in mouse. (**b–c**) Representative confocal image at the center of a thalamic injection site showing all cell nuclei (DAPI, blue), neurons (NeuN, red), and virally labeled cells (eGFP, green), shown individually in **b**, and overlaid in **c**. (**d**) The fraction of total cells infected at the center of an injection site (n = 17 green bar, mean ± s.d.). The fraction of total cells that are neurons at the center of an injection site (n = 5: red bar, mean ± s.d.). (**e**) The fraction of neurons infected at the center of an injection site (n = 5: yellow bar, mean ± s.d.). (**f–g**) Representative confocal image at the center of a thalamic co-injection of two viruses showing all cell nuclei (DAPI, blue), cells infected by virus expressing the fluorophore tdTomato (red), and cells infected by virus expressing the fluorophore eGFP (green), shown individually in **f**, and overlaid in **g**. (**h**) Quantification of the fraction of total cells expressing one or both co-injected viruses, showing that total infectable cell population is larger than a single injection will infect on average (n = 4, mean ± s. d.). All scale bars are 50 μm.

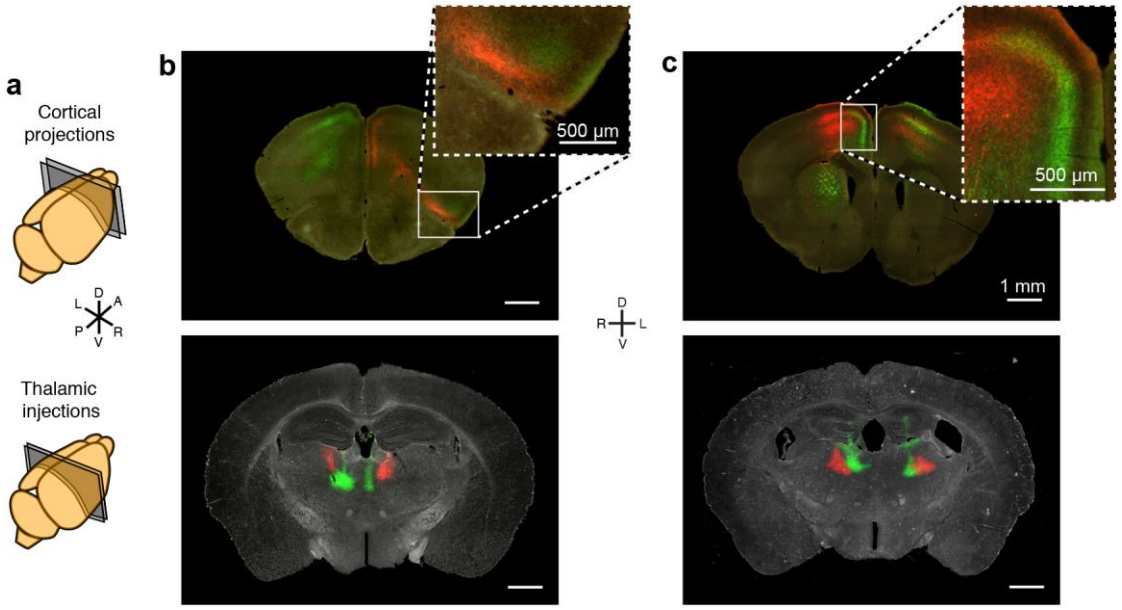

Supplementary Figure 2

Two-color injections reveal topographic projection information.

(**a**) Illustration showing the section locations for images in **b** and **c**. (**b–c**) Example thalamus sections showing injection sites (bottom), and example cortical sections showing thalamocortical projections (top). The insets for **b** and **c** show a zoomed image of juxtaposed red and green projections. (**b**) The green injection in the right hemisphere projects to AI, while the red injection, which originated lateral to the green injection in the thalamus, sends axonal projections to more medial brain structures, including LO, which is immediately adjacent to AI. (**c**) The green injection in the left hemisphere projects primarily to cortical layers 1 and 2/3 in the cingulate cortex, while the red injection projects to all cortical layers of motor cortex immediately adjacent to the green projections, largely maintaining separation of their respective projection fields. All scale bars are 1 mm unless otherwise specified.

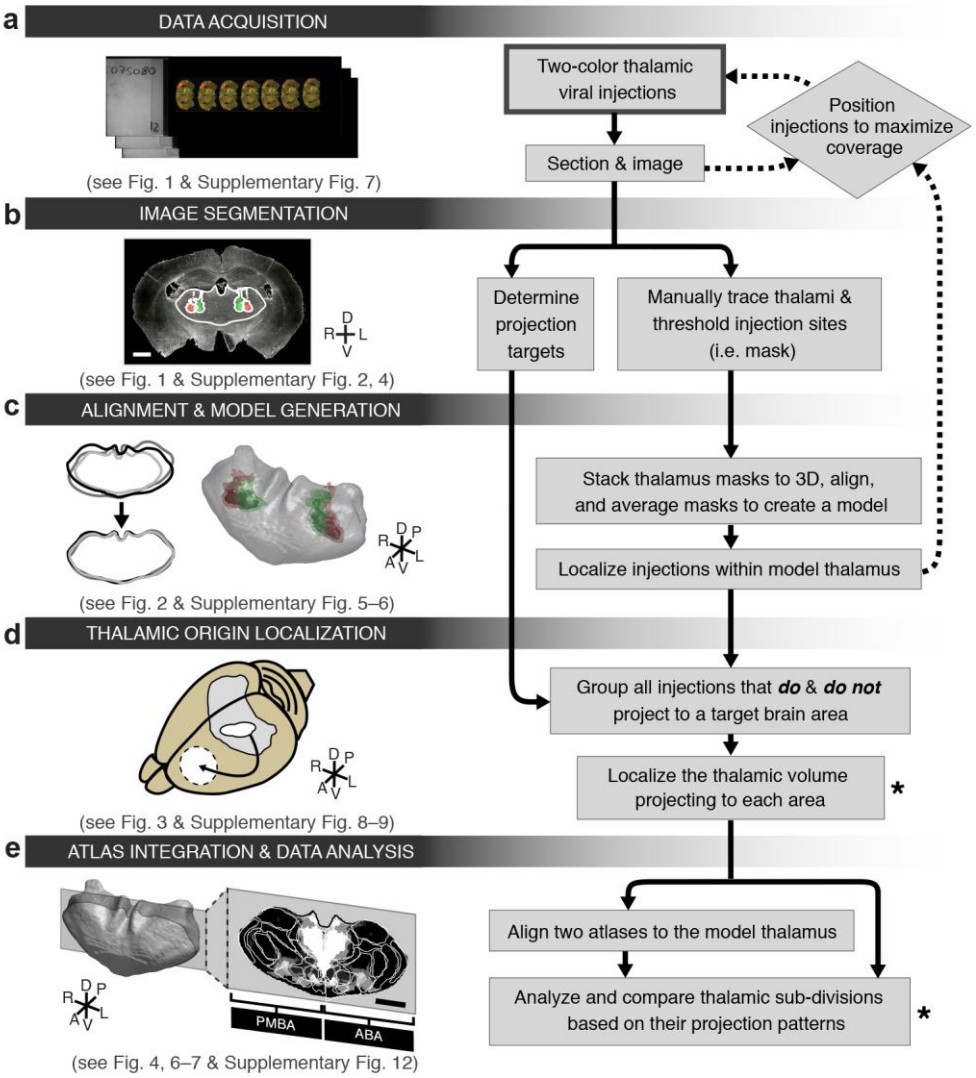

Supplementary Figure 3

Schematic flow chart of anatomical tracing and analysis methods.

(**a**) Data acquisition: the entire thalamus is labeled with small viral injections, sectioned, and imaged at a 0.5 µm/pixel resolution. (**b**) Image segmentation and projection identification: binary masks of the thalamus and injection sites are created and cortical sub-regions are scored for the presence or absence of projections. (**c**) Data alignment and model generation: thalamus masks are rotated, sheared, scaled and aligned. The aligned masks are then averaged to create a model thalamus. All injection sites are subsequently mapped onto the model thalamus. (**d**) Thalamic origin localization: injection site location and projection information are combined to define the precise thalamic volume projecting to a region of interest. (**e**) Atlas integration and data analysis: thalamic output patterns are determined using either the classic nuclear subdivision of the Paxinos Mouse Brain Atlas (PMBA) and the Allen Brain Atlas (ABA), or through atlas independent projection analyses. The thick-lined box indicates the starting point of the experiment while asterisks indicate the major output of the data analysis. All scale bars are 1 mm.

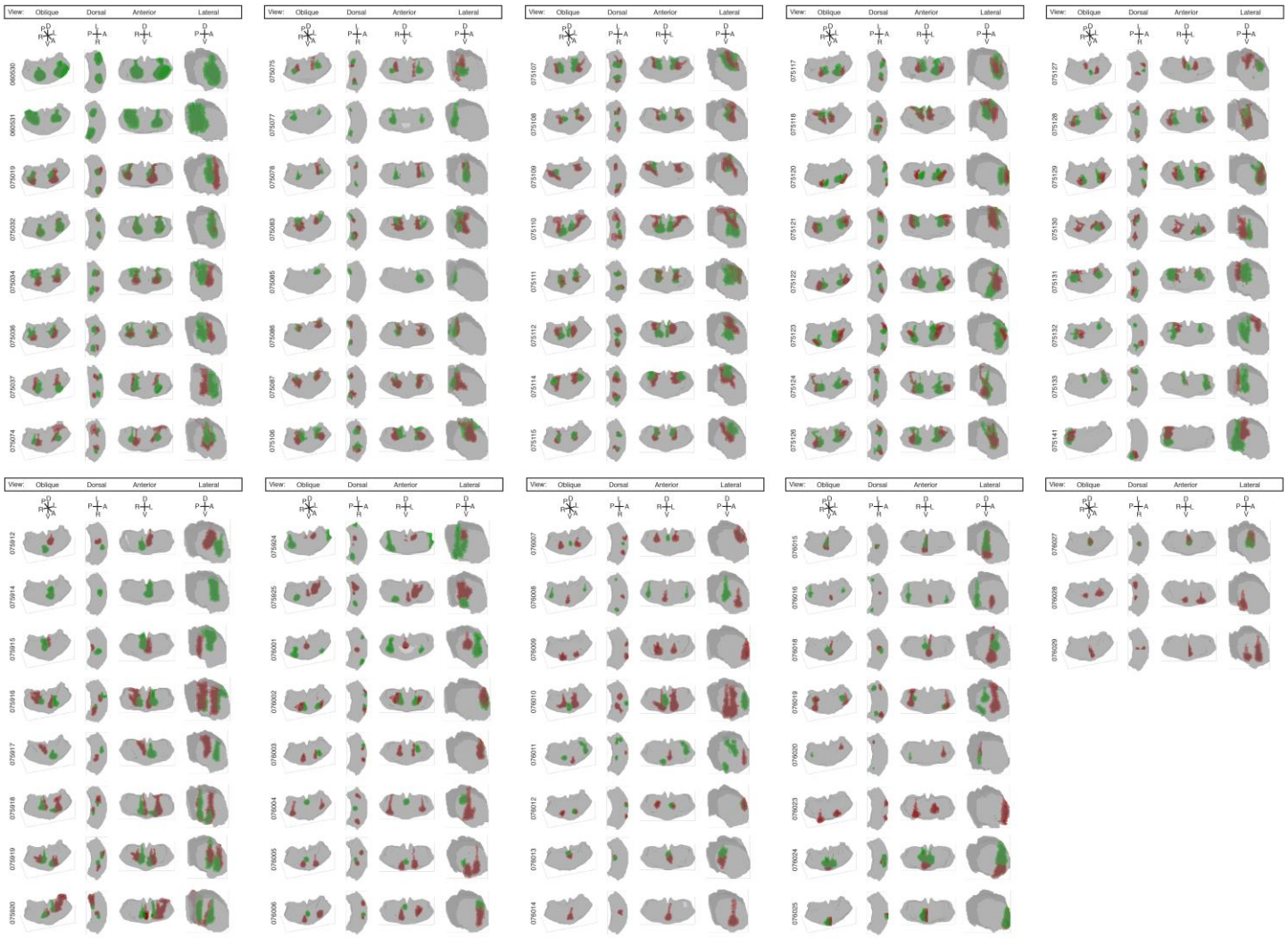

Supplementary Figure 4

3D rendering of the thalami and corresponding viral injections of all 75 experimental brains.

Each row shows an oblique, dorsal, anterior, and lateral view of an individual experimental thalamus. Axis descriptions are shown for the first thalamus only. Viral injection sites (red/green fluorescence) are shown within the traced thalamus from each brain (gray). A darker center of each injection site represents the eroded 'core' of the injection as described in **Figure 1**. For a higher resolution version of this figure, please visit http://digitalcollections.ohsu.edu/projectionmap.

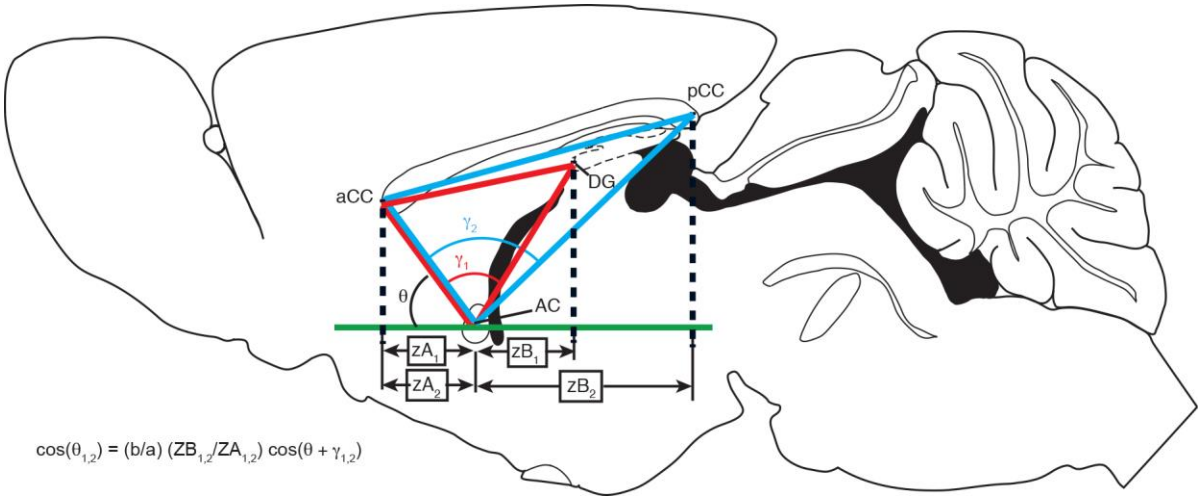

Supplementary Figure 5

Slice angle estimation from anatomical landmark positions.

Slice angle is estimated using the slice locations of several landmarks. In each case, the landmarks form a triangle, either between the medial anterior corpus callosum (aCC), the anterior commissure (AC) and the anterior dentate gyrus (DG) (i = 1, red) or between the aCC, the AC, and the medial posterior corpus callosum (pCC) (i = 2, blue). Assuming the sides of the triangle are fixed and proportional to the atlas dimensions (ABA), we can define the angles γ_1 and γ_2, using the red and blue coordinates, respectively. The fixed sides of the red triangle constrain the relationship between zA_1 and zB_1 so that θ_1 (estimated cutting angle) can be found from slice locations zA_1 and zB_1 only (and similarly for θ_2). θ_1 and θ_2 were determined from the equation numerically, and the final cutting angle tilt estimation was the average of θ_1 and θ_2. Baseline θ_{ABA} values for ABA sections were measured from ABA landmark locations, and brains with $|\theta_C - \theta_{ABA}| > 2°$ were subjected to rotation correction.

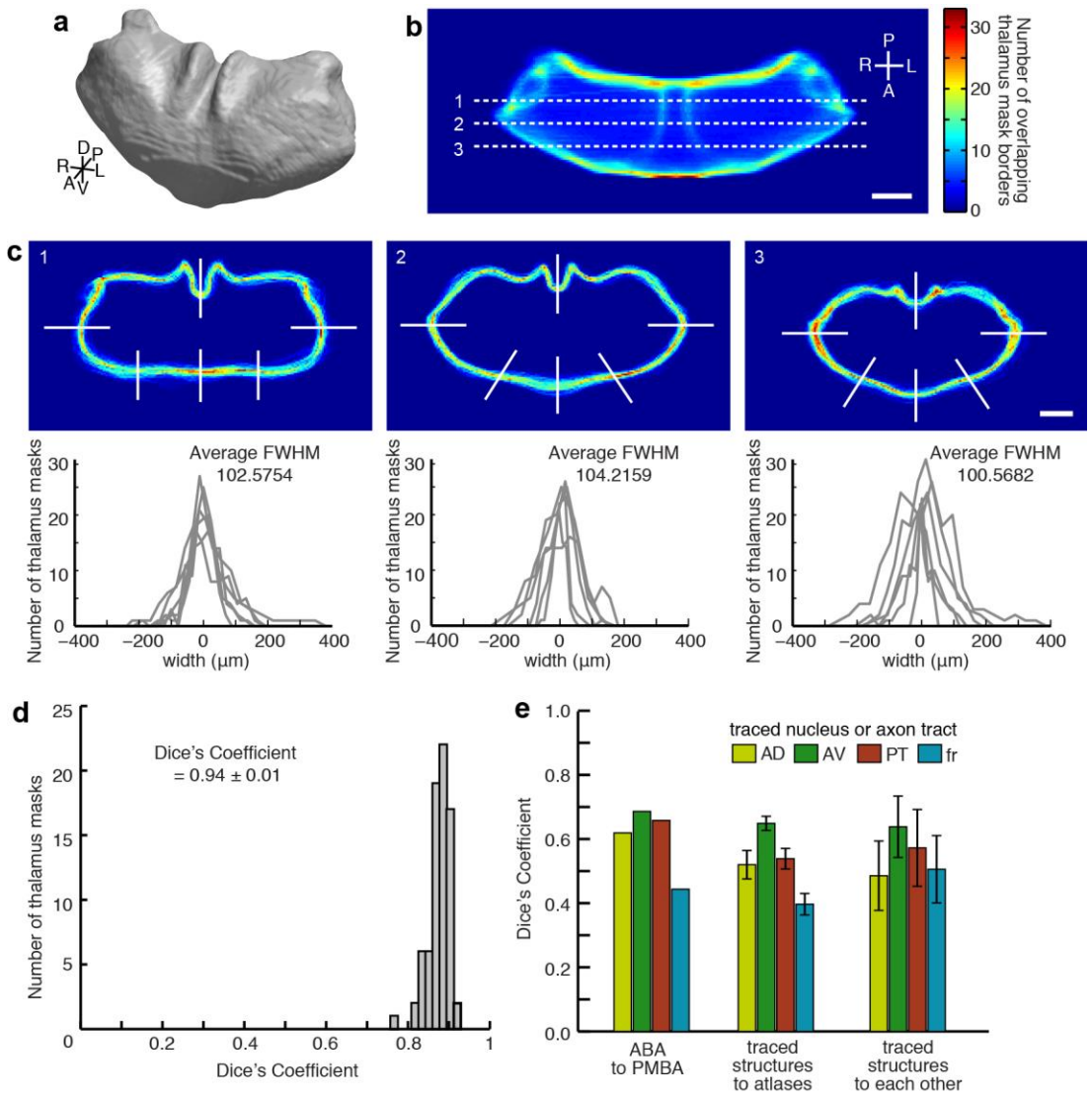

Supplementary Figure 6

Variability across thalamus masks and cytoarchitecturally identifiable thalamic structures.

(**a**) 3D rendering of the model thalamus created by averaging individual thalamus masks (oblique view). (**b**) To assess thalamus mask variability, we created the 3D perimeter matrix *P*, which contains the sum of the perimeter voxels of all 75 experimental thalamus masks. Color map indicates the summed projection of *P* along dorsal-ventral axis. (**c**) The top panels show x-y cross sections through *P* at the z locations marked in panel **b** as 1, 2, and 3. The bottom panels show profiles at the locations indicated in top of each panel (white lines). Full width half maximum (FWHM) across all profiles is 102 ± 51 μm (mean ± s.d.). (**d**) Histogram of Dice's Similarity Coefficient for individual thalamus masks. Individual thalamus masks are highly similar to the model thalamus, with Dice's coefficient between individual masks and the model $D = 0.94 \pm 0.01$ (mean ± s.d.). (**e**) Four cytoarchitecturally identifiable thalamic structures (AD, AV, PT, and fr) were manually traced in five experimental brains and two atlases (PMBA and ABA), as described in **Figure 2b–c**. Dice's Similarity Coefficient is plotted to compare the identified structures in two separate atlases (left, n = 2), to compare the atlases to the experimentally traced structures (middle, n = 5, mean ± s.d.), and to compare the experimentally traced structures to each other (right, n = 10, mean ± s.d.). All scale bars are 1 mm.

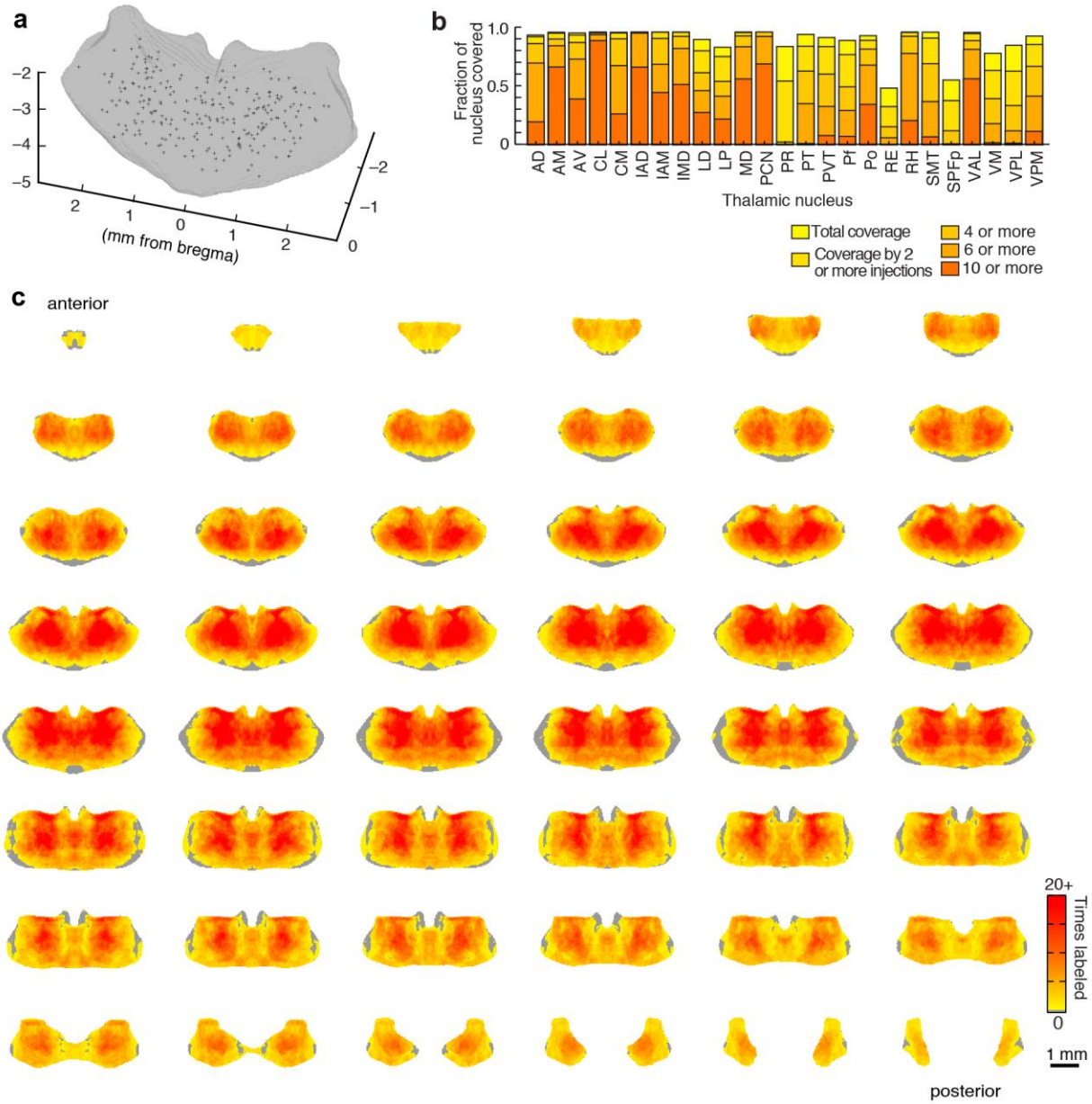

Supplementary Figure 7

Full characterization of injection coverage within the model thalamus.

(**a**) Oblique view of the model thalamus (gray) with the center of mass of all 254 injection sites (black crosses). (**b**) Coverage of the thalamus broken down by nucleus. Fraction of each nucleus covered by at least 1, and at least 2, at least 4, at least 6 and at least 10 injections, showing that the entire volume of most thalamic nuclei is sampled at least 4 times. (**c**) Full coverage montage of the thalamus. Coronal slices through the thalamus starting at –0.155 mm posterior to bregma, and continuing in 50 µm increments to the posterior end of the thalamus. The color scale indicates the number of times an independent injection labeled a given location of the thalamus.

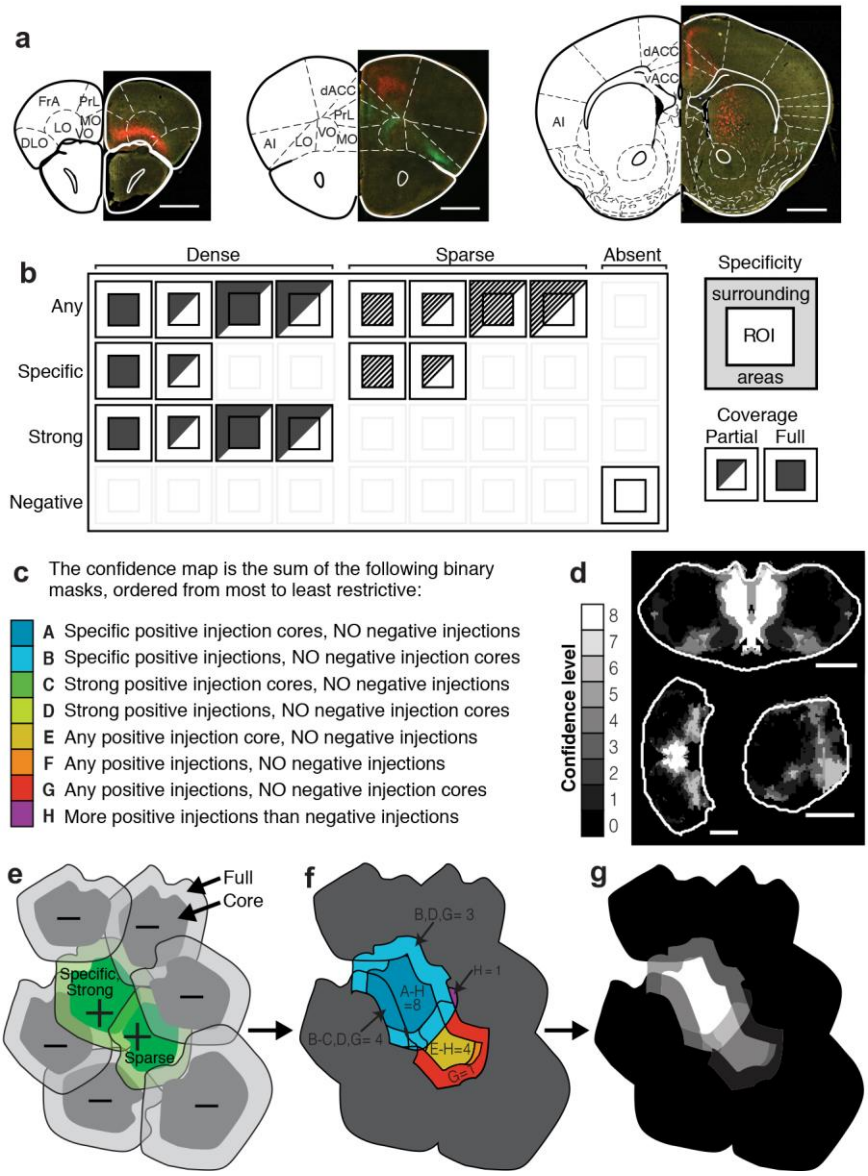

Supplementary Figure 8

Projection scoring criteria and injection grouping method.

(**a**) PMBA sections with corresponding mouse brain images on the right, showing example projection distributions within several regions of interest (ROIs) in the frontal cortex. (**b**) Diagram of projection scoring criteria: strength (either dense or sparse labeling within the ROI) and specificity (either projections locally confined to the ROI or projections that also go to surrounding areas). Partial or full coverage within the ROI was also scored, but differences in thalamic origin profiles were not found (data not shown). (**c**) Description of each binary mask created by grouping the scored injections as described. (**d**) Example confidence map created by summing the binary masks created in **c**, where each mask adds a value of 1, and all masks (A–H) must be true at a given point to reach a confidence level of 8 (white). (**e–g**) Illustration of how a confidence map is created. (**e**) Illustration of eight injections and their corresponding score, showing the full injection as well as the eroded core. (**f**) Sample of the binary masks created from panel **e** as described in panel **c**. (**g**) Confidence map created from panel **f** as described in panel **d**. All scale bars are 1 mm.

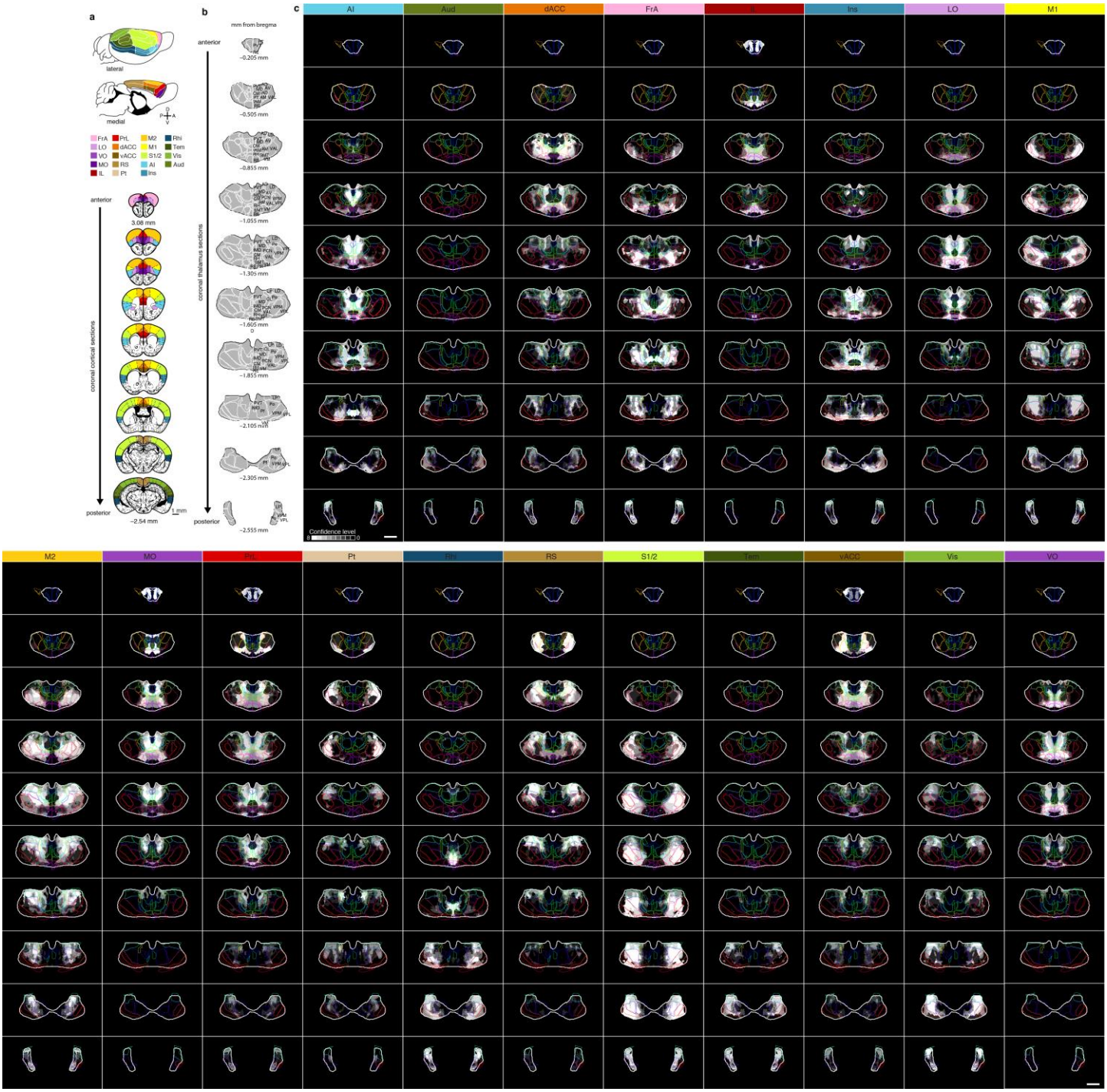

Supplementary Figure 9

Full confidence maps for the thalamic origin of all cortical projections.

(**a**) The cortical areas examined (modified from PMBA[25] and ref 47) are shown. Lateral and medial whole brain views (top) and coronal sections from anterior to posterior (bottom). (**b**) Reference coronal sections for the confidence maps shown in panel **c**, with the bregma coordinates noted in the anterior-posterior axis. (**c**) Each column contains the confidence map for a given cortical sub-region, arranged alphabetically, with coronal sections corresponding to those in panel **b**. The confidence maps (gray scale) show the thalamic origin of projections to nineteen cortical sub-regions: FrA, LO, VO, MO, IL, PrL, vACC, dACC, RS, Pt, M2, M1, S1/2, AI, Ins, Rhi, Tem, Vis, and Aud. The outline of the model thalamus is shown in white for each section, and the aligned nuclei from PMBA (left) and the ABA (right),

are overlaid as colored outlines (nuclei labeled for AI only). All scale bars are 1 mm. For a higher resolution version of this figure, please visit http://digitalcollections.ohsu.edu/projectionmap.

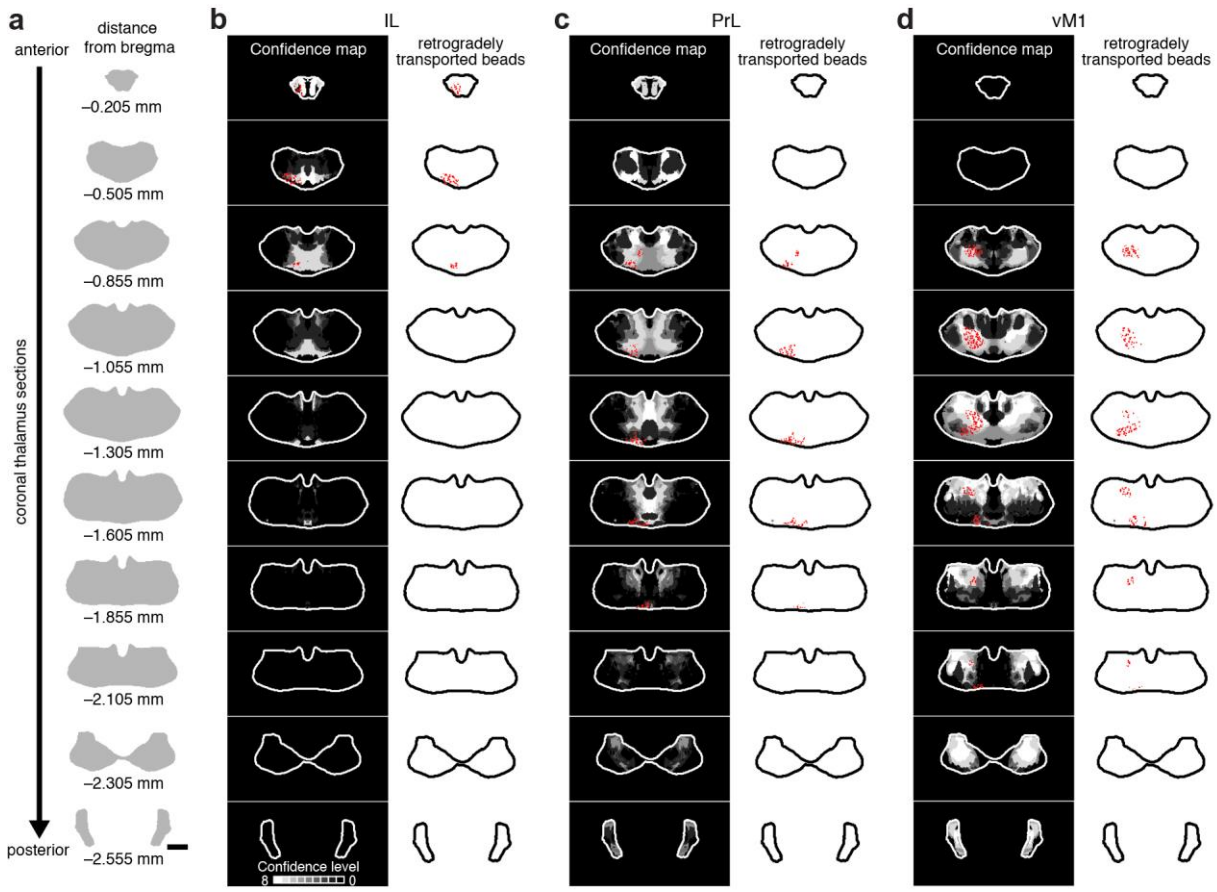

Supplementary Figure 10

Retrograde bead injections fall within the thalamic volume predicted by the confidence maps.

(**a**) Reference coronal sections for the confidence maps shown in panel **b–d**, with the bregma coordinates noted in the anterior-posterior axis. (**b–d**) Thalamic location of retrogradely transported beads 3 days after injection in the indicated cortical sub-region (total of 10 mice injected and 3 analyzed in detail). The confidence maps (gray scale, left: see **Fig. 3** for detail) show the predicted thalamic origin of projections to three cortical sub-regions; (**b**) IL, (**c**) PrL, and (**d**) vM1. The locations of beads that were retrogradely transported from the indicated cortical region are overlaid on the left of each confidence map section (red dots), and shown independently on the right. The outline of the model thalamus is shown for each section (left: white, right: black). All scale bars are 1 mm.

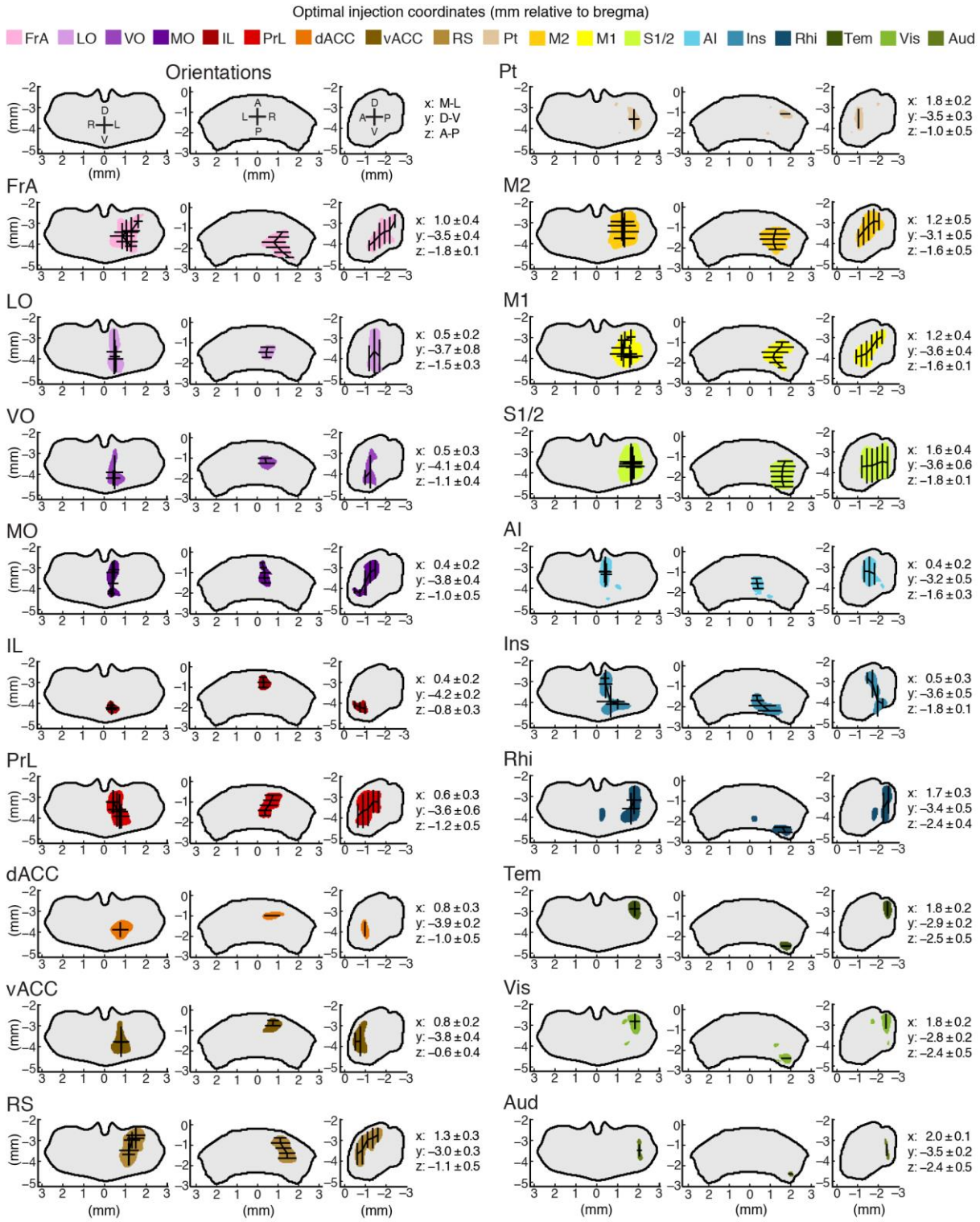

Supplementary Figure 11

Optimal injection coordinates used to target specific thalamocortical projections.

Optimal injection coordinates, i.e. the most probable location to inject in order to target a specific thalamocortical pathway, were determined for each of the 19 cortical sub-regions: FrA, LO, VO, MO, IL, PrL, vACC, dACC, RS, Pt, M2, M1, S1/2, AI, Ins, Rhi, Tem,

Vis, and Aud. The orientation of each thalamus view is indicated in the top left column. The colored areas for each cortical projection sub-region denote the location with the highest probability to label those projections. A single set of coordinates is listed to the right of each cortical sub-region. All coordinates are shown in millimeters relative to bregma.

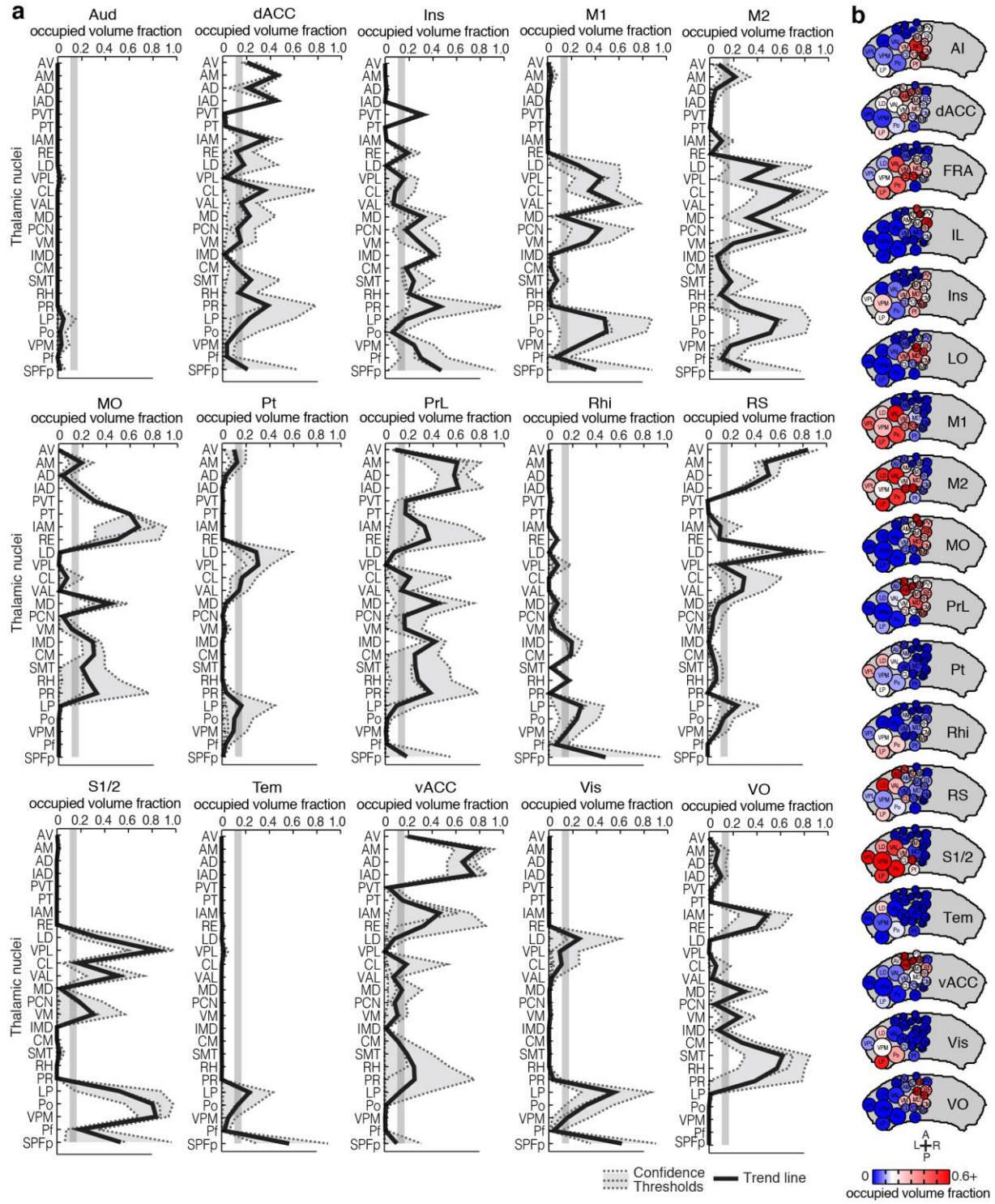

Supplementary Figure 12

Nuclear localization of the thalamic origins of cortical projections.

(**a**) The fractions of each thalamic nucleus projecting to Aud, dACC, Ins, M1, M2, MO, Pt, PrL, Rhi, RS, S1/2, Tem, vACC, Vis, and VO are shown in three confidence levels (dashed lines) with their average (black line). Vertical gray line: the inflection point in the color scale used in panel **b**. (**b**) Spatial representations of all nuclei projecting to the each cortical sub-region, arranged alphabetically. Circle diameters correspond to the relative size of each nucleus and their positions correspond to their relative center-of-mass location within

the thalamus in the anterior-posterior and medial-lateral axes. Auditory cortex is not shown because we did not identify any projections from our injections.

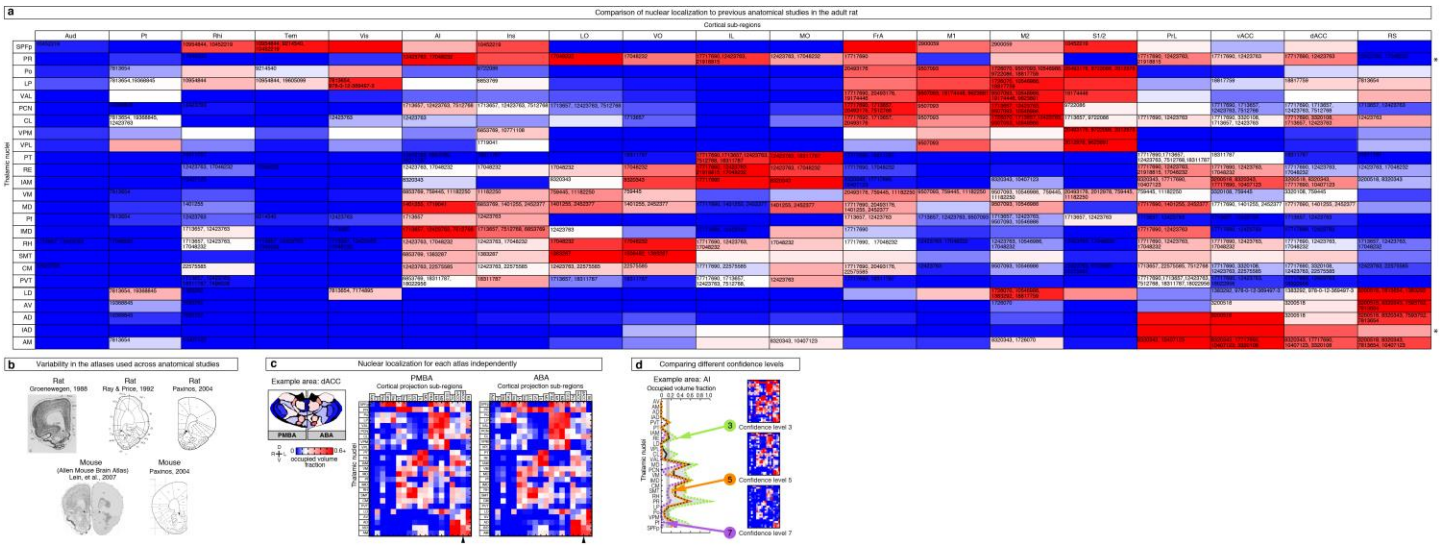

Supplementary Figure 13

Localizing and verifying the thalamic nuclear origins of cortical projections.

(**a**) Comparison of our thalamic nuclear localization data in mouse to previous studies of thalamocortical projections in the adult rat. Nuclear localization map as described in **Figure 6e**, overlaid with the PubMed ID #'s for publications with evidence for the corresponding thalamocortical projection. Some specific projections are inferred from data presented in the publications. Asterisks indicate thalamic nuclei with little or no anatomical data in the rat literature. (**b**) Examples of several atlases used in literature to classify cortical sub-regions in the literature. (**c**) Comparison of nuclear localization maps for two atlases separately (ABA and PMBA). Left: Coronal section showing the nuclear subdivisions from the PMBA (left) and ABA (right). Nucleus colors indicate the fraction of each nucleus covered by the dACC confidence map described in **Figure 6**. Right: Aggregate nucleus coverage map of all thalamocortical projections using the PMBA and ABA separately. Nuclei (rows) and cortical sub-regions (columns) are ordered as in **Figure 6e**. The ABA and PMBA specific maps were averaged to produce **Figure 6e**. (**d**) Comparison of nuclear localization maps for separate confidence levels (using averaged atlases). Left: The fraction of each nucleus projecting to AI, shown for three confidence levels (dashed lines, 3, 5 and 7) and their average (black line) as described in **Figure 6**. Right: Nucleus localization maps for the three confidence levels. Nuclei (rows) and cortical sub-regions (columns) are ordered as in **Figure 6e**. All three maps are averaged to produce **Figure 6e**. For a higher resolution version of this figure, please visit http://digitalcollections.ohsu.edu/projectionmap.

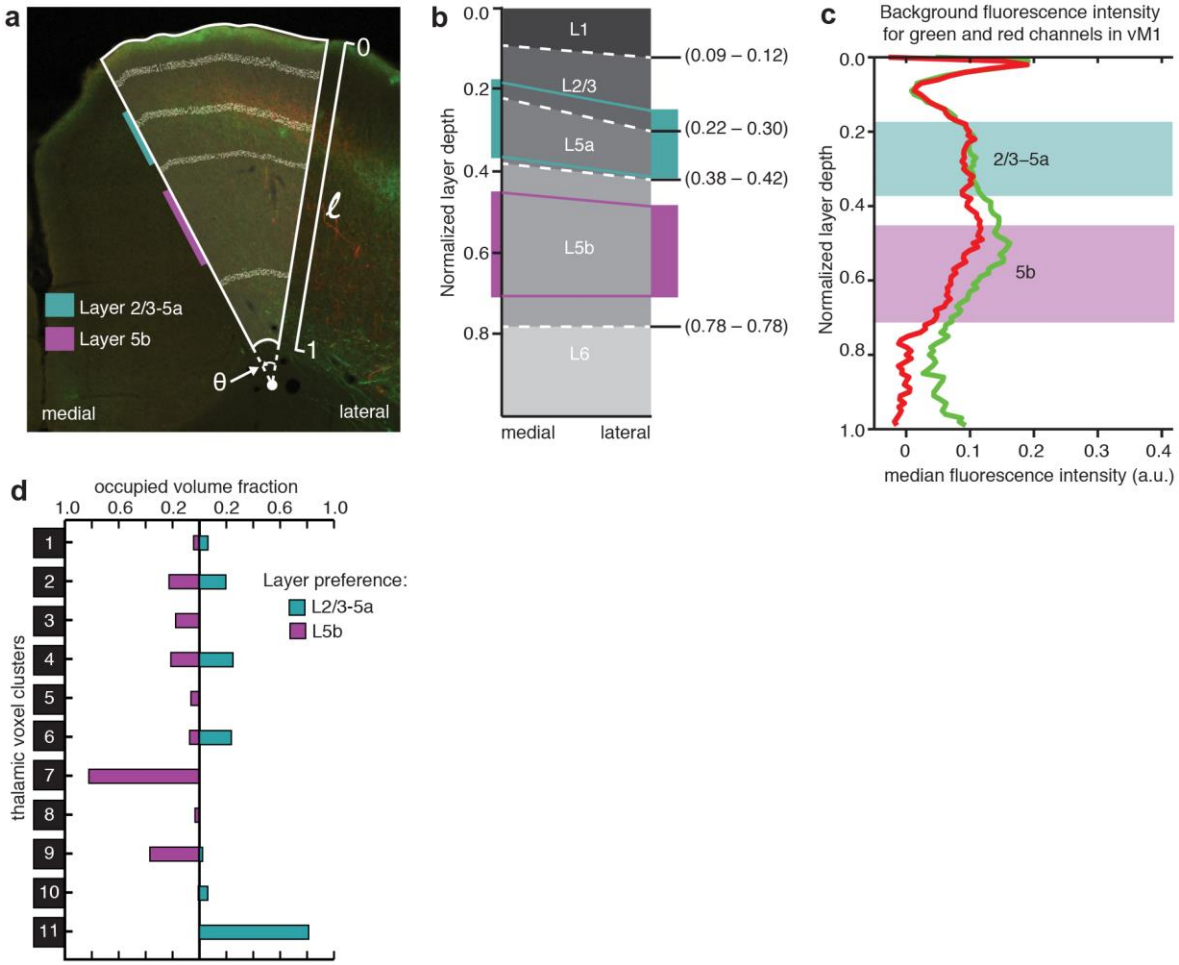

Supplementary Figure 14

vM1 layer boundaries and background fluorescence.

(**a**) Representative vM1 image showing the layer boundaries. Relative thicknesses of cortical layers in vM1 vary from the lateral edge to the medial edge. The parameters used in calculations are indicated: *l*: relative cortical depth (0 at the pia and 1 at white matter); θ: the angel of the ROI. Horizontal lines: layer boundaries. The depth regions analyzed for layer preferential projections are indicated (color bars). (**b**) Schematic of layer depth variation from medial to lateral edge. The boundaries at the medial and lateral edges are based on previous characterizations. At other radial positions, the layer boundaries were linearly interpolated from the lateral to medial edges. The boundaries were normalized to the cortical layer depth. Colored regions and lines indicate the regions analyzed for layer preferential projections. (**c**) Background florescence along the normalized cortical depth. All fluorescence was first mapped to the corresponding layer depth at the medial edge before being binned and averaged. Background fluorescence was calculated as the median fluorescence at a depth bin across brains manually determined not to have projections from the thalamus to vM1. (**d**) Assessment of 11 thalamic voxel clusters' layer-preferential projections to vM1. The clusters were determined as described in **Figure 4**. The occupied fraction of each thalamic voxel cluster containing layer-preferential projections to L2/3–5a (cyan) or 5b (magenta) of vM1 is plotted as a fraction of total cluster volume.